Patient-Specific Hemodynamics of the Descending Aorta: Combination of CFD and 4D Flow-Sensitive MRI

A. F. Stalder[1], Z. Liu[2], M. Markl[1], J. Hennig[1], and J. Korvink[2]

[1]Dept. of Diagnostic Radiology - Medical Physics, University Hospital Freiburg, Freiburg, Germany, [2]Dept. of Microsystems Engineering, University of Freiburg, Freiburg, Germany

Introduction: The assessment of vascular function parameters such as blood flow, pressure or wall shear stress is continuously gaining interest for the diagnosis and treatment of cardiovascular diseases (1-2). In this context, flow-sensitive 4D MRI has demonstrated its potential for 3D blood flow visualization and flow parameter estimation (3). Studies have shown that some flow and wall parameters can directly be estimated from MR phase-contrast (PC-MRI) velocity measurements (4-6). But the estimation of large velocity ranges, e.g. retrograde flow dynamics or derived parameters such as Wall Shear Stress (WSS) remains limited by the spatio-temporal resolution of PC-MRI. This has been a motivation for the use of Computational Fluid Dynamics (CFD) with realistic geometric and inflow boundary conditions that can be derived from MRI or CT measurements. However, blood flow in the arteries is particularly complex, including phenomena such as non-Newtonian rheology, compliant and moving arteries and fluid-wall interactions. Those aspects are often neglected due to limited knowledge on those phenomena and/or high complexity of computational models. The aim of the presented method was to combine 4D flow-sensitive MRI and CFD into a single framework (Fig. 1) in order to enhance blood flow estimations. Consequently, 4D flow-sensitive MRI was used for the finite element model definition (geometry and boundary conditions) as well as for verification of the CFD solution.

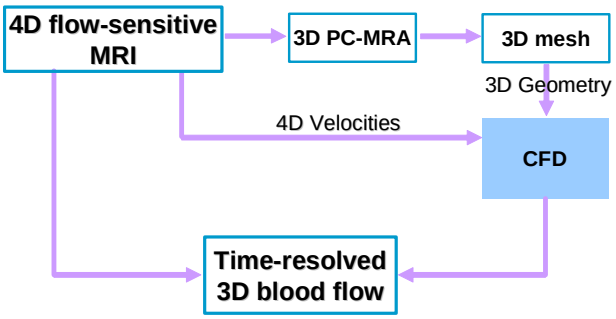

Fig. 1 Time-resolved 3D blood flow using combined 4D flow-sensitive MRI and CFD.

Methods: MR data acquisition was performed at 3T (Trio, Siemens, Germany) on a young healthy volunteer after injection of a blood pool contrast agent (MS 325, Vasovist; Schering AG, Berlin, Germany). The thoracic aorta was imaged using a respiration controlled and ECG gated 3D rf-spoiled gradient echo sequence with 3-directional velocity encoding (spatial resolution: 2.82 x 1.67 x 3.5 mm^3, temporal resolution: 48.8 ms, venc: 1.5 m/s) (3). From this time-resolved 3D dataset, a phase contrast angiography (PC-MRA) was calculated (7) and was used for segmentation of the descending aorta using level-set active contours (8) after manual initialization with at least one seed sphere. After adjustment of propagation, curvature and advection (gradient-based) forces, a smooth geometry of the descending aorta was extracted with subvoxel resolution (Fig. 2a) and a 3D volumetric mesh with 15'000 tetrahedral elements was derived. The flow-sensitive 4D MRI data was used to define inflow boundary conditions which exactly matched the *in-vivo* situation. In addition, null-pressure at the outlet plane and no-slip on the vessel wall were used as boundary conditions. CFD was performed using a commercial finite element solver (Comsol 3.3a, http://www.comsol.com) based on a direct linear solver (PARDISO) and with anisotropic diffusion stabilization. Blood was assumed to be incompressible with a density of 1050 kg/m^3 and a dynamic viscosity of 0.005 Pa·s. The model was solved over 4 cardiac cycles, using the complete 3D MR velocity field as initialization.

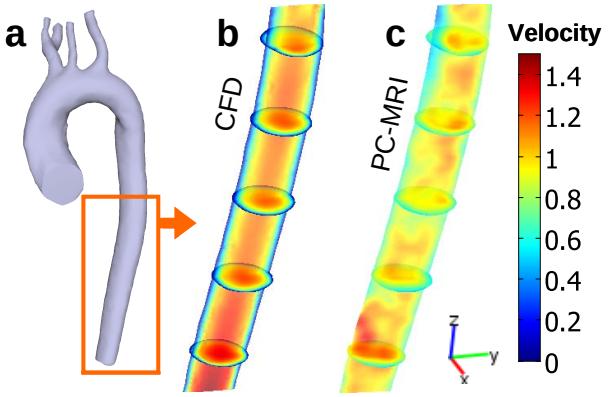

Fig. 2 a: Section of the descending aorta **b-c:** velocity at peak systole derived from CFD (b) and PC-MRI (c).

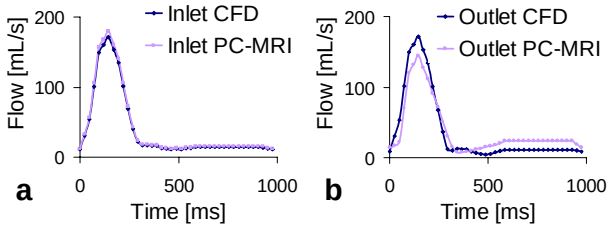

Fig. 3 Inflow (a) and Outflow (b) from CFD and PC-MRI.

Results: The vessel boundaries were successfully segmented (Fig. 2a) by placing 4 seed spheres (1 per branch). The velocity field could be effectively simulated using CFD (Fig. 2b) and compared to the velocity field from PC-MRI spatially (Fig. 2b-c) and temporally (Fig. 3). Moderate spatial agreement was observed during peak systole between CFD (Fig. 2b) and PC-MRI (Fig. 2c). Temporal flow correlation in shape and amplitude was excellent at the inlet (Fig. 3a) and good at the outlet (Fig. 3b). Times to peak were identical up to the temporal resolution.

Discussion: The results of this study show for the first time a direct comparison of 3D flow characteristics simulated by CFD and measured *in-vivo* by flow-sensitive MRI based on an integration of both modalities into the same framework. A good agreement was found between PC-MRI and CFD based on realistic PC-MRI boundary conditions at the inlet. Partial volume effect from MR measurement is likely to be one source of error explaining the spatial discrepancies between CFD and PC-MRI. The flow discrepancies at the outlet might be due to the geometry simplifications, i.e. neglected compliance by using rigid walls and neglected small branches flowing out of the aorta. Nevertheless, the overall good temporal agreement, with identical time to peak flow between CFD and PC-MRI, supports the validity of the CFD model and the assumption of blood incompressibility. Combination of 4D flow-sensitive MRI with CFD not only allows calculating patient-specific flow simulations from a single MR measurement but may also offer additional reciprocal validation possibilities. While CFD simulations may introduce errors by using simplified blood flow models (e.g. rigid and/or no-slip walls, Newtonian rheology), PC-MRI suffers from measurement errors (e.g. Maxwell terms, non-linearity of gradients or acceleration effects). Combination of those 2 complementary approaches has the potential to refine *in-vivo* 3D flow measurements and may result in more accurate quantification of *in-vivo* hemodynamics and eventually enhance the understanding of the complex arterial blood flow.

References: 1. Richter Y. et al., Circulation 113:2679-2682 (2006) 2. Cheng C. et al, Circulation 113:2744-2753 (2006) 3. Markl M. et al, J Magn Reson Imaging 25:824-831 (2007) 4. Wentzel J.J. et al, J Am Coll Cardiol 45:846-54 (2005) 5. Oyre S, Magn Reson Med 40:645-655 (1998) 6. Yang G.-Z. et al, Magn Reson Med 36:520-526 (1996) 7. Bock J. et al. Proc. 15th ISMRM p. 3138 (2007) 8. Yushkevich P.A. et al. Neuroimage 31:1116-1128 (2006)

Acknowledgements: Deutsche Forschungsgemeinschaft: Grant HE 1875/18-1; Bundesministerium für Bildung und Forschung: Grant 01EV0706